

# Bounds on absorption and thermal radiation for arbitrary objects

Sean Molesky, Weiliang Jin, Prashanth S. Venkataram, and Alejandro W. Rodriguez  
*Department of Electrical Engineering, Princeton University, Princeton, New Jersey 08544, USA*

We derive bounds on angle-integrated absorption and thermal radiation for arbitrary bodies (of prescribed material susceptibility and domain size) that account for both the per-volume limit on polarization response set by the optical theorem and geometry specific finite size constraints imposed by the interplay of material and radiative losses. We then consider these bounds in a number of common settings, comparing against prior limits as well as nearly optimal structures discovered using topology optimization, and show that they properly capture the transition from the volume scaling characteristics of deeply subwavelength objects (nanoparticle radius or thin film thickness) to the area scaling of the blackbody in the ray optics limit.

Motivated by the increasing control of light offered by micro and nanoscale structuring [1, 2], impetus to find upper bounds on absorption and thermal radiation analogous to the blackbody limits for geometries that violate the assumptions of ray optics (nanoparticles [3], thin films [4], photonic crystals [5, 6], etc.) has steadily grown over the past several decades. It is now long established that the absorption cross-section of a compact object can be much greater than its geometric area [7–12] (resulting in “super-Planckian” emission), and that thin films can achieve very high absorptivity via surface texturing [13, 14]. A limit applicable for all length scales and materials could both provide insight into these representative phenomena and guide efforts in related application areas such as LEDs [15, 16], photovoltaics [17–19], and photon sources [20–22].

Development of bounds for arbitrary objects, Fig. 1, has primarily followed from two overarching strategies: modal decompositions based on quasi-normal, Fourier and/or multipole expansions [23–31], relating an object’s absorption cross-section to the number of excitable optical modes (radiation channels), or conservation principles, utilizing energy [32, 33] and/or spectral sum rules [34–36] to determine the achievable optical response of a medium. Separately, each of these approaches present challenges for use in photonic design. Modal decompositions tend to inherently incorporate the specific size and shape characteristics of a body, and hence require enumeration and characterization of the relevant participating modes [24, 37, 38]. Although fundamental considerations (transparency, constraints on energy, object sizes, etc.) have been employed in this regard [26, 31, 39], present cut-offs do not tightly bound potential properties when considering an arbitrary compact geometry, particularly when applied to metallic nanoparticles and antennas [25, 33, 40]. Conversely, conservation principles, which provide bounds on a medium’s polarization response limited by intrinsic dissipation, naturally reproduce the volumetric scaling of absorptivity for deeply subwavelength objects (and are highly accurate in the special case of weak polarizability for this regime [33]). However, due to the implicit reliance of

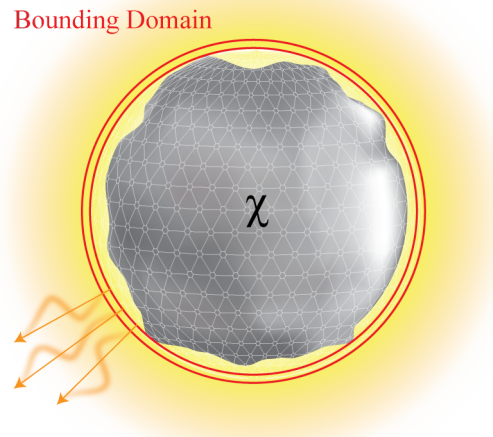


FIG. 1. **Schematic of investigation.** To what extent does the material response (electric susceptibility  $\chi$ ), and a bounding domain (volume  $V$ ) constrain the thermal emission and integrated absorption characteristics of an arbitrary object?

these bounds on uniform fields and their neglect of finite size effects, the same volumetric scaling persists for all length scales. As a consequence, conservation bounds rapidly become too loose when applied beyond quasi-static settings, yielding unphysical divergences with both increasing object size and material response.

In this article, we derive bounds on thermal radiation and absorption that combine these two approaches, linking the impact of material response with the influence of an object’s size and shape on scattering. The result is applicable to objects of any size, exhibiting a smooth transition in absorptivity from the volume scaling of the quasi-static regime to the area scaling of macroscopic ray optics. Further, the bounds always asymptotically approach the blackbody limit regardless of material response (when all characteristic lengths are large) and diverge logarithmically—rather than quadratically—with material response for compact domains. Finally, we compare the present results to prior bounds and structures

discovered using topology optimization, realizing a variety of examples (both metallic and dielectric) that nearly achieve the predicted limits.

## RESULTS

**Derivation**—Thermal radiation for any object at a given angular frequency  $\omega$  and temperature  $T$

$$H(\omega, T) = \Pi(\omega, T) \Phi(\omega) \quad (1)$$

can be expressed in terms of its scattering characteristics through the  $\mathbb{T}$  operator (reviewed in Appendices) and the vacuum Green function  $\mathbb{G}^{\text{vac}}$  [41] as

$$\Phi = \frac{2}{\pi} \text{Tr} [\text{Asym} \{ \mathbb{G}^{\text{vac}} \} (\text{Asym} \{ \mathbb{T} \} - \mathbb{T}^\dagger \text{Asym} \{ \mathbb{G}^{\text{vac}} \} \mathbb{T})]; \quad (2)$$

where  $\Pi(\omega) = \hbar\omega / (\text{Exp}(\beta\hbar\omega) - 1)$  with  $(\beta = k_B T)$  is the Planck energy of a harmonic oscillator,  $\text{Tr}[\dots]$  denotes the trace, and  $\text{Asym} \{ \mathbb{T} \} = (\mathbb{T} - \mathbb{T}^\dagger) / 2i$  denotes the asymmetric component of an operator. By Kirchhoff's law [42] (2) also equals any object's angle integrated absorption. (Another derivation of (2) is given in our recent work on bounds for radiative heat transfer [43].) To constrain the magnitude of this expression we begin by recalling two properties of the involved operators. First, the optical theorem requires the singular values of the  $\mathbb{T}$  operator to be bounded above by the *material figure of merit*,

$$\zeta = \frac{|\chi(\omega)|^2}{\text{Im}[\chi(\omega)]}, \quad (3)$$

i.e.  $\|\mathbb{T}\|_2 \leq \zeta$ . This fact, previously derived in Ref. [33] through variational optimization, sets a physical limit on the magnitude of the polarization that can arise for any incident field. Second, because  $\text{Asym} \{ \mathbb{G}^{\text{vac}} \}$  is real-symmetric positive-definite, it can be expressed via a singular value decomposition as

$$\text{Asym} \{ \mathbb{G}^{\text{vac}} \} = \sum_i \rho_i |\mathbf{q}_i\rangle\langle\mathbf{q}_i|. \quad (4)$$

Together, these two considerations (see Appendices) are sufficient to show that any optimal  $\mathbb{T}$  operator should be diagonalizable in the basis of singular vectors of  $\text{Asym} \{ \mathbb{G}^{\text{vac}} \}$  and have purely imaginary eigenvalues:

$$\mathbb{T} = \sum_i i\tau_i |\mathbf{q}_i\rangle\langle\mathbf{q}_i|, \quad (5)$$

with  $\tau_i \in [0, \zeta]$ . Applying (5) to (2) and maximizing the contribution of each singular value subject to the material constraint yields

$$\begin{aligned} \Phi_{\text{opt}} &= \frac{1}{2\pi} \sum_i \Theta(2\zeta\rho_i - 1) \\ &+ \frac{2}{\pi} \sum_i \rho_i \zeta (1 - \rho_i \zeta) \Theta(1 - 2\zeta\rho_i), \end{aligned} \quad (6)$$

where  $\Theta$  is the Heaviside step function. Based on the criterion  $\rho_i \zeta \geq 1/2$ , each index of (6) produces either the maximum entropy flow per channel (Landauer bound) contribution of  $1/4$  [44, 45], or the material limited contribution of  $\rho_i \zeta (1 - \rho_i \zeta)$ , with saturation of absorption occurring under the rate matching condition of equal dissipative and radiative loss rates. A proof that (6) is domain monotonic is given in Appendices.

**Analysis**—While (6) is straightforward to compute for any geometry of interest (elongated cylinders, disks, spheres, extended films, etc.) using numerical methods [46, 47], it is also well approximated by a simplified model that is amenable to semi-analytic evaluation for highly symmetric domains. Specifically, for the representative case of a spherical domain (and homeomorphisms thereof), the singular values of  $\text{Asym} \{ \mathbb{G}^{\text{vac}} \}$  display a natural split: up to some length scale dependent index they are essentially constant, then, after a brief transitional knee, they begin to decay as a geometric factors over factorials. (Corroborating details for this statement are included in Appendices.) For small enough  $\zeta$  or domain volume, the knee is small and the contribution of the tail region is insubstantial. As such, there is typically little difference between evaluation of (6) with the set of optimal  $\{\tau_i\}$ , and evaluation with a single optimized  $\tau_{\text{sc}}$ . Within this *scalar approximation*, the optimal flux corresponding to a domain of volume  $V$  is given by

$$\begin{aligned} \Phi_{\text{sc}}(\tau_{\text{sc}}, V) &= \tau_{\text{sc}} \int_V d\mathbf{r} \text{Asym} \{ \mathbb{G}^{\text{vac}}(\mathbf{r}, \mathbf{r}) \} \\ &- \tau_{\text{sc}}^2 \iint_V d\mathbf{r} d\mathbf{r}' \text{Asym} \{ \mathbb{G}^{\text{vac}}(\mathbf{r}, \mathbf{r}') \}^2. \end{aligned} \quad (7)$$

The linear coefficient of  $\tau_{\text{sc}}$  in (7) is the local density of states integrated over the volume of the domain. By itself, this whole term is maximized when  $\tau_{\text{sc}} = \zeta$ , and under this saturation of the material response, it is larger than either the full form (6) or (7). Interestingly, it is also the result of applying the per-volume (geometry independent) optical response limit described in Ref. [33] to angle integrated absorption over a region, and similar to the local density of states light trapping bound given in Ref. [32]. Due to these connections with prior literature,

$$\Phi_{\text{Born}}(V) = \zeta \int_V d\mathbf{r} \text{Asym} \{ \mathbb{G}^{\text{vac}}(\mathbf{r}, \mathbf{r}) \} \quad (8)$$

serves as a useful comparison for our present investigation, and is subsequently referred to as a *Born bound*, owing to its neglect of higher-order scattering present in the second term. For any combination of parameters

$$\Phi_{\text{sc}} \leq \Phi_{\text{opt}} \leq \Phi_{\text{Born}}. \quad (9)$$

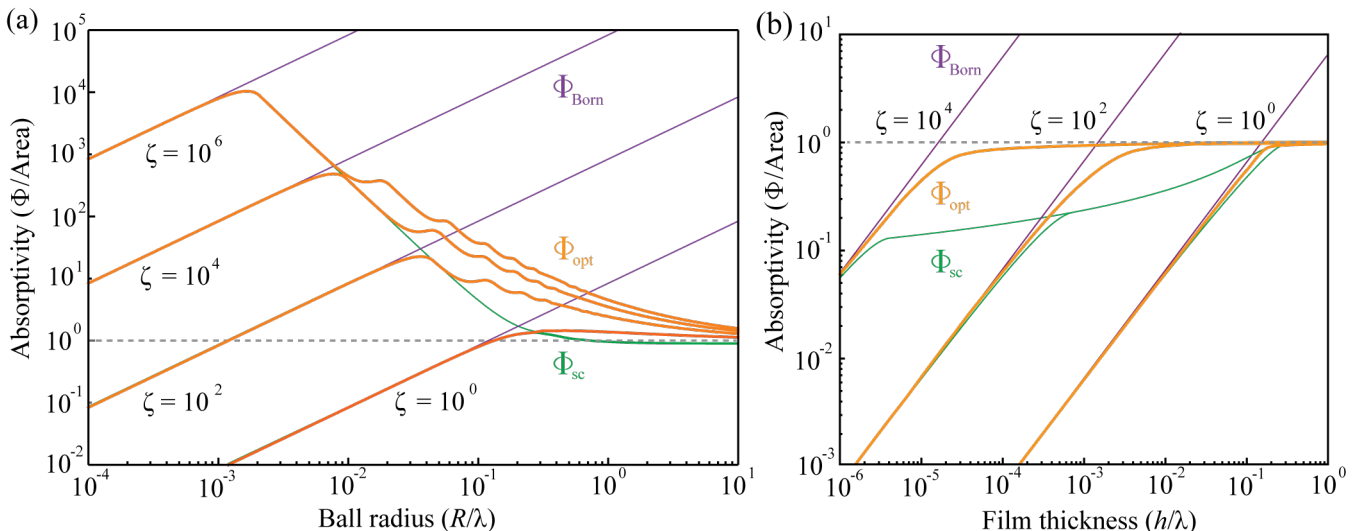


FIG. 2. **Upper bounds on angle-integrated absorption and thermal radiation for compact and extended bodies.** The figure shows the absorptivity ( $\Phi$  normalized by area  $A$ ) bounds  $\Phi_{\text{opt}}$  (orange lines) and  $\Phi_{\text{Born}}$  (purple lines), along with the approximation  $\Phi_{\text{sc}}$  (green lines), for several values of the material figure of merit  $\zeta = |\chi|^2/\text{Im}[\chi]$  at a fixed wavelength  $\lambda$ . These quantities are shown as a function of the wavelength normalized radius  $R$  of an enclosing sphere (a), and thickness  $h$  of a semi-infinite film (b). Even for small characteristic lengths ( $\{R, h\} \leq 0.1\lambda$ )  $\Phi_{\text{opt}}$  is orders of magnitude smaller than  $\Phi_{\text{Born}}$ . Notably, high absorptivity is seen for certain subwavelength domains (nanoparticles and thin films).

The quadratic coefficient of  $\tau_{\text{sc}}^2$  in (7),

$$C_{\text{corr}}(V) = \iint_V d\mathbf{r} d\mathbf{r}' A_{\text{sym}} \{G^{\text{vac}}(\mathbf{r}, \mathbf{r}')\}^2, \quad (10)$$

which we designated as the *domain correlation*, is less familiar, but still intuitive. The presence of strong polarization currents, necessary for strong per-volume absorption, leads to size dependent scattering and radiative losses; in turn, these effects decrease possible absorption. The competition between these two terms mirrors known features of absorption and scattering cross-sections for highly subwavelength objects (e.g. metallic antennas): absorption  $\propto V$  and scattering  $\propto V^2$  [24, 28]. (6) and (7) are natural extensions, with the  $(\rho_i \zeta)^2$  terms representing per-channel scattering losses due to finite object sizes.

**Examples**—Evaluations of (6), (7) and (8) for two prototypical domains are shown in Fig. 2. Due to the high symmetry of these geometries, semi-analytic evaluation is manageable and carried out in Appendices. We begin with panel (a) investigating spherically bounded volumes. In the quasi-static regime,  $R/\lambda \ll 1$ , (6) is almost entirely determined by the first singular value  $\rho_1$  of  $A_{\text{sym}} \{G^{\text{vac}}\}$  (the monopole). Yet, although ( $\forall i \neq 1$ )  $\rho_1/\rho_i \gg 1$ ,  $\rho_1$  is still small compared to  $\zeta$  for the (realistic) material factors shown here. This results in absorption being dominated by material dissipation. Accordingly,  $\Phi_{\text{opt}} \approx \Phi_{\text{sc}} \approx \Phi_{\text{Born}}$  so that, normalizing by the surface area of the sphere, all three forms scale  $\propto 2^3 \pi \zeta R / (3\lambda)$ .

As the domain grows, so too do the values of  $\rho_i$ , and

the agreement of  $\Phi_{\text{opt}}$  and  $\Phi_{\text{sc}}$  with  $\Phi_{\text{Born}}$  breaks down. From the perspective of radiative emission, finite size or “wave” effects (scattering, interference, correlation, etc.) eventually preclude the possibility that every position in a domain can act as an independent perfect emitter saturating the material figure of merit. These effects cause the normalized magnitudes of  $\Phi_{\text{opt}}$  and  $\Phi_{\text{sc}}$  to drop, regularizing the volumetric divergence of  $\Phi_{\text{Born}}$ . For a fixed radius, as discussed in Appendices, the growth of (6) with  $\zeta$  compared to (8) is also greatly reduced.

The differences caused by these corrections become increasingly pronounced as the domain grows comparable or greater than the wavelength,  $R \gtrsim 0.5\lambda$ . Essentially, as the domain expands, an increasing number of channels (higher-order multipoles) become saturated. This leads to the steps seen in  $\Phi_{\text{opt}}$ , and for values greater than  $R \approx 0.2\lambda$  causes the domain correlation to tend rapidly to the asymptotic value  $C_{\text{corr}}(R) \approx 2^3 \pi^5 (R/\lambda)^4$ . Selecting the optimum  $\tau_{\text{sc}}$  (in this limit) of  $\tau_{\text{sc}} = (\pi^2 R/\lambda)$  yields the asymptotic scalar approximation

$$\Phi_{\text{sc}}(R) \approx \frac{2^3}{3^2} 4\pi (R/\lambda)^2, \quad (11)$$

which is 8/9 of a perfect spherical absorber in the ray optics limit. Although  $\Phi_{\text{opt}}$  and  $\Phi_{\text{sc}}$  do not perfectly agree in the intermediate range of  $10^{-2} \lesssim R/\lambda \lesssim 1$ , as a result of the previously mentioned knee in  $\rho_i$ , their overall characteristics are largely similar. In the large  $R/\lambda$  limit,  $\Phi_{\text{opt}}$  always asymptotes to a perfect spherical absorber, i.e. the blackbody limit applied to a ball, independent of the chosen material.

Analogous results for an extended body (infinite area

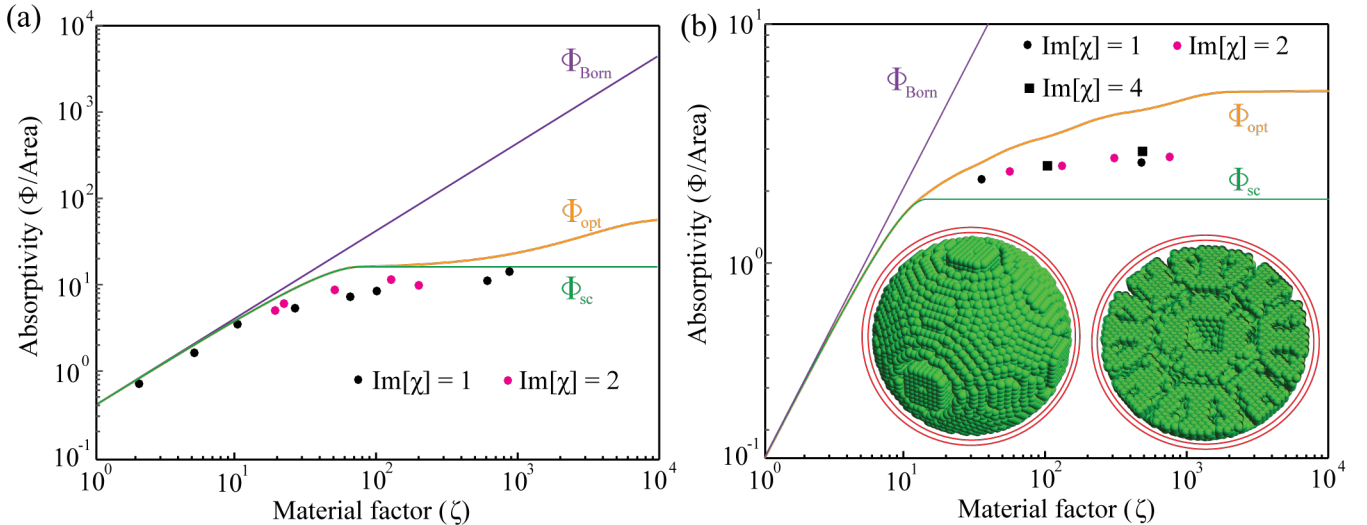


FIG. 3. **Comparison of bounds with geometries discovered by inverse design.** The figure plots the absorptivity ( $\Phi$  over area  $A$ ) of structures discovered using gradient topology optimization for a variety of metallic (a) and dielectric (b) materials of susceptibility  $\chi$ , characterized by the material figure of merit  $\zeta = |\chi|^2 / \text{Im}[\chi]$ . For comparison the bounds  $\Phi_{\text{opt}}$  (6) and  $\Phi_{\text{Born}}$  (8), and the scalar approximation  $\Phi_{\text{sc}}$  (7) are also depicted. For panel (a), all structures are bound by a ball of radius  $R = 0.05\lambda$ . For panel (b), the confining domain is a ball of  $R = 0.5\lambda$ . The inset provides a visualization of the structure (exterior and  $xy$ -plane cut) for the rightmost black square. The observation that optimized structures come within factors of unity from our bounds and the scalar approximation provides case evidence of the tightness of (6) and usefulness of (7).

$A$  and finite thickness  $h$ ) are shown in Fig. 2 (b). In this situation, as derived in Appendices, one finds that

$$C_{\text{corr}}(V) = A c(h),$$

so that

$$\Phi_{\text{sc}}(h)/A = 2^3 \pi (h/\lambda) \tau_{\text{sc}} - c(h) \tau_{\text{sc}}^2. \quad (12)$$

The optimal value of  $\tau_{\text{sc}}$  is then given by  $\tau_{\text{sc}} = \min\{\zeta, 2\pi^2 (h/\lambda) / c(h)\}$ , where  $c(h)$  is a monotonic integral trigonometric function of thickness. As before, in the deeply subwavelength limit  $h \ll \lambda$  one recovers  $\Phi_{\text{Born}}$ , as absorptivity is closely approximated by the internal density of states; in the limit of large thickness  $h \gg \lambda$  (ray optics) both  $\Phi_{\text{sc}}$  and  $\Phi_{\text{Born}}$  become independent of material and reproduce the blackbody limit for a solid angle of  $4\pi$  steradians. Some disagreement between (6) and (7) is observed for “intermediate” thicknesses,  $h/\lambda \lesssim 10^{-1}$ . However, in the Fourier description of  $\text{Asym}\{\mathbb{G}^{\text{vac}}\}$ , this difference results from oscillations in the singular values, which are damped as the thickness increases. The finding that  $\Phi_{\text{opt}}$  does not disqualify the possibility of near unity absorptivity in extremely thin films is tacitly supported by a growing number of studies in 2D materials and meta-surfaces [48–50].

Case evidence for the tightness of (6) is presented in Fig. 3. Using a gradient topology (density) optimization design algorithm [2, 51], see Appendices, two of the major features of  $\Phi_{\text{opt}}$  for a spherically bounded domain are explored: the separation of  $\Phi_{\text{Born}}$  from  $\Phi_{\text{opt}}$  and  $\Phi_{\text{sc}}$ , panel (a)  $R/\lambda = 0.05$ , and the separation of  $\Phi_{\text{opt}}$  from

$\Phi_{\text{sc}}$ , panel (b)  $R/\lambda = 0.5$ . As was previously remarked by Miller et al. [33], in the quasi-static regime  $\Phi_{\text{Born}}$  is attained for a plane wave polarized along the axis of an ellipsoidal metallic particle, given a properly chosen aspect ratio. For small values of  $\zeta$  this ratio is near unity and resonant metallic structures ( $\text{Re}[\chi] \approx -3$ ) matching all three bounds are easily discovered. As  $\zeta$  moves to moderate values the aspect ratio required for an ellipsoidal particle to match  $\Phi_{\text{Born}}$  becomes increasingly extreme. Due to our choice of a spherical boundary, the discovered structures begin to deviate considerably from  $\Phi_{\text{Born}}$ , but continue to come within a factor of 2 of  $\Phi_{\text{opt}}$  for  $\zeta$  as large as  $10^3$ . Past this material figure of merit, numerical issues impede our present algorithms and it remains to be seen to what extent the roughly order of magnitude headroom allowed by  $\Phi_{\text{opt}}$  is accessible ( $\zeta \lesssim 10^5$  is attained by some metals in the infrared [52]). The data trend suggests that  $\Phi_{\text{sc}}$  may be more realistic for such a deeply subwavelength domain. Intuitively, the dominant singular vectors of  $\text{Asym}\{\mathbb{G}^{\text{vac}}\}$  show qualitatively similar radial characteristics, and this makes creating multiple distinct polarization responses difficult.

Results for the larger domain, Fig. 3 (b), nevertheless prove that  $\Phi_{\text{sc}}$  can be surpassed. One such example is depicted in the right inset (full view and  $xy$ -plane cut), corresponding to the rightmost black square of the plot. In agreement with the assumptions made in reaching (6), the  $\mathbb{T}$  operator for this dielectric structure ( $\chi = 20 + 4i$ ,  $\Phi = 0.60 \Phi_{\text{opt}}$ ) is found to be nearly diagonal in the basis of  $\text{Asym}\{\mathbb{G}^{\text{vac}}\}$  and have almost completely imaginary

eigenvalues. Supporting data and additional details are given in Appendices. (Note that metals in non-spherical domains may nearly saturate the bounds for wavelength-scale volumes.)

## DISCUSSION

There are a number of practical points that should be considered when making use of (6), or comparing to prior work. First,  $\Phi_{\text{opt}}$  represents a bound on thermal emission and integrated absorption for a given domain and  $\zeta$  factor. By choosing different geometries (elongated cylinders, disks, spheres, extended films, etc.) and material parameters, (6) can be applied to any desired context, but the connection to the confining volume is an essential feature. Second, there is no universal guarantee of tightness. Beyond the demonstrated agreement of the bounds with known quasi-static and ray optics asymptotics, the only a priori guarantee we have given is domain monotonicity. In all likelihood, there are certain volumes and material parameters where the value of  $\Phi_{\text{opt}}$  will be considerably larger than the true  $\Phi$  of any practical structure. This caveat is especially relevant to the results of Fig. 3 concerning objects with small characteristic length scales, which remain prime candidates for realizing extremely high-field intensities, absorption cross sections, and super-Planckian emission in the present bounds. Next, while the example domains we have explored are highly symmetric, we stress that the approach itself does not rely on any symmetry, or for that matter connectedness, of the domain. Numerical singular value decomposition is agnostic to these features. As previously suggested,  $\Phi_{\text{opt}}$  can be interpreted as the extension of prior multipole analysis to general domains with the crucial addition that an upper bound is set on the number modes which may possibly contribute through a combination of the pseudo-rank of the imaginary part of the vacuum Green function ( $\text{Asym}\{\mathbb{G}^{\text{vac}}\}$ ) and the material figure of merit ( $\zeta$ ) (3). We foresee this rank revealing capability possibly providing a number of benefits for future practical design and optimization studies. Finally, while differences do exist, much of what has been developed in this manuscript is applicable to the related problem of light extraction (from incident planewaves or individual dipolar emitters) with applications to solar cells, light-emitting diodes, and single-photon emitters.

In summary, using purely algebraic arguments, we have amalgamated two previously considered approaches to derive limits on thermal emission and optical absorption (modal analysis and passivity). This has led to bounds (6) that are simple to compute and incorporate two of the primary considerations of actual design: the material the device will be made of and the volume within which it will be confined. The bounds are applicable to objects of any size, agreeing with known large and small

length scale limits, and display a more realistic dependence (logarithmic versus quadratic divergence) on the material figure of merit  $|\chi|^2/\text{Im}(\chi)$  than previous absorptivity limits for compact objects. Using a topology optimization algorithm, we have also provided sample structures for a number of different materials (metals and dielectrics) that nearly achieve the predictions of the bounds, giving case evidence for their tightness.

## ACKNOWLEDGMENTS

This work was supported by the National Science Foundation under Grants No. DMR-1454836, DMR 1420541, DGE 1148900, the Cornell Center for Materials Research MRSEC (award no. DMR1719875), the Defense Advanced Research Projects Agency (DARPA) under agreement HR00111820046, and the National Science and Engineering Research Council of Canada under PDF-502958-2017. The views, opinions and/or findings expressed herein are those of the authors and should not be interpreted as representing the official views or policies of any institution.

## APPENDICES

**T operator properties**—Following the Lippmann-Schwinger approach to scattering [53], the  $\mathbb{T}$  operator is formally defined through the self-consistent equation

$$\mathbf{E} = \mathbf{E}_{\text{inc}} + \mathbb{G}^{\text{vac}}\mathbb{V}\mathbf{E}, \quad (13)$$

as

$$\mathbb{T}^{-1} = \mathbb{V}^{-1} - \mathbb{G}^{\text{vac}}, \quad \mathbf{J} = \mathbb{T}\mathbb{V}^{-1}\mathbf{J}_{\text{inc}}, \quad (14)$$

with the “inc” subscript denoting an initial (freely incident) current (field),  $\mathbb{G}^{\text{vac}}$  the vacuum Green function, and  $\mathbb{V}$  a generalized electromagnetic susceptibility. A lack of any subscript indicates total field quantities. The singular value condition quoted in the main text is derived by applying these definitions to the passivity condition that the power scattered by a medium must always be a positive quantity. That is,  $P_{\text{scat}} = P_{\text{ext}} - P_{\text{abs}} \geq 0$ . Using the fact (Kong [54]) that

$$P_{\text{ext}} = \frac{k_o}{2Z} \text{Im} [\langle \mathbf{E}_{\text{inc}} | \mathbb{V} | \mathbf{E} \rangle], \quad (15)$$

$$P_{\text{abs}} = \frac{k_o}{2Z} \text{Im} [\langle \mathbf{E} | \mathbb{V} | \mathbf{E} \rangle] \quad (16)$$

with  $k_o = \omega/c$ ,  $Z = \sqrt{\mu_0/\epsilon_0}$ , given an arbitrary initial current source  $|\mathbf{J}_{\text{inc}}\rangle$ , passivity then implies that

$$\begin{aligned} \text{Im} [\langle \mathbf{J}_{\text{inc}} | \mathbb{V}^{-1\dagger} \mathbb{T} \mathbb{V}^{-1} | \mathbf{J}_{\text{inc}} \rangle] &\geq \\ \text{Im} [\langle \mathbf{J}_{\text{inc}} | \mathbb{T}^\dagger \mathbb{V}^{-1\dagger} \mathbb{V}^{-1} \mathbb{T} \mathbb{V}^{-1} | \mathbf{J}_{\text{inc}} \rangle], &\quad (17) \end{aligned}$$

and in turn,

$$\|\text{Asym}\{\mathbb{T}\} - \mathbb{T}^\dagger \text{Asym}\{\mathbb{V}^{-1*}\}\mathbb{T}\|_2 \geq 0. \quad (18)$$

Making the assumption of a local, linear, isotropic, non-magnetic media so that  $\mathbb{V} = \chi(\omega)\mathbb{I}$ , the singular values of  $\mathbb{T}$  are thus bounded by the material factor quoted in the main text. An alternative derivation of this bound was obtained by Miller et al.[33] based on passivity, known as the optical theorem, and variational optimization.

The above properties also validate the act of decoupling the singular values of  $\text{Asym}\{\mathbb{G}^{\text{vac}}\}$  (the collection  $\{\rho_i\}$ ) from the actual volume of the object used in deriving (6) (additional details below).  $\mathbb{T}$  takes free electric fields and produces total polarization currents—which are automatically confined to the material body. Hence, in applying (2) the domain of  $\text{Asym}\{\mathbb{G}^{\text{vac}}\}$  may freely be taken to be larger than that of the object (the domain of  $\mathbb{T}$ ). Any mismatch between the domain of the object and the domain of  $\text{Asym}\{\mathbb{G}^{\text{vac}}\}$  technically reduces  $\|\mathbb{T}\|$  below (3), but accounting for this change simply produces a slightly stronger, more complex, version of (6).

**Optimal  $\mathbb{T}$  operator.**—The stated properties of an operator maximizing  $\Phi$  follow from considering (2) in terms of (4):

$$\begin{aligned} \Phi = \frac{2}{\pi} & \left( \sum_i \rho_i \left( \text{Im} [\langle \mathbf{q}_i | \mathbb{T} | \mathbf{q}_i \rangle] - \rho_i |\langle \mathbf{q}_i | \mathbb{T} | \mathbf{q}_i \rangle|^2 \right) \right. \\ & \left. - \sum_{\{(i,j)|i \neq j\}} \rho_i \rho_j |\langle \mathbf{q}_i | \mathbb{T} | \mathbf{q}_j \rangle|^2 \right). \end{aligned} \quad (19)$$

In this setting, consider  $\mathbb{T}$  as some operator in the space

$$\{\mathbb{T} \ni \|\mathbb{T}\|_2 \leq \zeta \ \& \ \text{Asym}\{\mathbb{T}\} \text{ positive semi-definite}\}, \quad (20)$$

and disregard all other physical constraints. Two characteristics of an optimal element in this set are clear. First,

$$(\forall i \neq j) \ \rho_i \rho_j |\langle \mathbf{q}_i | \mathbb{T} | \mathbf{q}_j \rangle|^2 \geq 0,$$

and so the appearance of any cross-terms ( $\langle \mathbf{q}_i | \mathbb{T} | \mathbf{q}_j \rangle$ ) will always decrease (19). Therefore, any optimal operator must be diagonalized in the basis of  $\text{Asym}\{\mathbb{G}^{\text{vac}}\}$ . Second, the angle of the response in the complex plane only influences the first (positive) piece of the above sum, and so the value of (19) will peak when

$$(\forall i) \ \text{atan} \left( \frac{\text{Im} [\langle \mathbf{q}_i | \mathbb{T} | \mathbf{q}_i \rangle]}{\text{Re} [\langle \mathbf{q}_i | \mathbb{T} | \mathbf{q}_i \rangle]} \right) = \frac{\pi}{2}.$$

Therefore, any optimal  $\mathbb{T}$  in (20) is simultaneously diagonalizable with  $\text{Asym}\{\mathbb{G}^{\text{vac}}\}$  and has purely imaginary eigenvalues.

**Domain monotonicity**— Let  $U$  be a subdomain of  $D$ , and

$$\begin{aligned} \text{Asym}\{\mathbb{G}_U^{\text{vac}}\} &= \sum_i u_i |\mathbf{u}_i\rangle \langle \mathbf{u}_i| \\ \text{Asym}\{\mathbb{G}_D^{\text{vac}}\} &= \sum_i d_i |\mathbf{d}_i\rangle \langle \mathbf{d}_i| \end{aligned} \quad (21)$$

be the vacuum Green functions for each of these volumes. Assume that these sums are finite. The first singular vector, corresponding to the largest singular value, is equivalent to the complex vector field  $\mathbf{f}(\mathbf{r})$  maximizing the integral

$$\iint_V d\mathbf{r} d\mathbf{r}' \mathbf{f}^*(\mathbf{r}) \text{Asym}\{\mathbb{G}^{\text{vac}}\}(\mathbf{r}, \mathbf{r}') \mathbf{f}(\mathbf{r}') \quad (22)$$

subject to the constraint,  $\int_V d\mathbf{r} \mathbf{f}^*(\mathbf{r}) \mathbf{f}(\mathbf{r}) = 1$ .

It is clear that moving to a larger volume is always favourable in this context. In the worst case  $\mathbf{f}(\mathbf{r})$  simply does not change. Hence, that the largest singular value of  $\text{Asym}\{\mathbb{G}^{\text{vac}}\}$  is domain monotonic. Now, suppose that all singular values up to  $i = N$  have been shown to be domain monotonic so that  $(\forall i \leq N) u_i \leq d_i$ , and consider  $i = N + 1$ . Recall that the  $N + 1$  singular vector  $|\mathbf{d}_{N+1}\rangle$  is defined by the property of maximizing  $\langle \mathbf{d}_{N+1} | \text{Asym}\{\mathbb{G}^{\text{vac}}\} | \mathbf{d}_{N+1} \rangle$  subject to the constraints  $(\forall i \leq N) \langle \mathbf{d}_i | \mathbf{d}_{N+1} \rangle = 0$  and  $\langle \mathbf{d}_{N+1} | \mathbf{d}_{N+1} \rangle = 1$ . Take  $\pi_U |\mathbf{d}_i\rangle$  to be the projection of  $|\mathbf{d}_i\rangle$  onto the subdomain  $U$ . If  $\sum_{i=1}^N \pi_U |\mathbf{d}_i\rangle$  spans  $\sum_{i=1}^N |\mathbf{u}_i\rangle$ , then we essentially return to the case of the first singular vector.  $|\mathbf{u}_{N+1}\rangle$  is orthogonal to all  $\pi_U |\mathbf{d}_i\rangle \ni i \leq N$ , and zero outside  $U$ . Therefore, it is orthogonal to all  $|\mathbf{d}_i\rangle \ni i \leq N$ . Since  $\langle \mathbf{u}_{N+1} | \text{Asym}\{\mathbb{G}_D^{\text{vac}}\} | \mathbf{u}_{N+1} \rangle = \langle \mathbf{u}_{N+1} | \text{Asym}\{\mathbb{G}_U^{\text{vac}}\} | \mathbf{u}_{N+1} \rangle$ , with the added freedom of the additional volume we must have  $d_{N+1} \geq u_{N+1}$ . If  $\sum_{i=1}^N \pi_U |\mathbf{d}_i\rangle$  does not span  $\sum_{i=1}^N |\mathbf{u}_i\rangle$ , then some elements of  $\{|\mathbf{u}_i\rangle \ni i \leq N\}$  are orthogonal to all  $\pi_U |\mathbf{d}_i\rangle$ . Select one such vector and denote it as  $|\mathbf{u}_\alpha\rangle$ . Since  $u_\alpha \geq u_{N+1}$ , by the preceding argument  $d_{N+1} \geq u_{N+1}$ .

**Singular values for balls**—To derive the singular values of  $\text{Asym}\{\mathbb{G}^{\text{vac}}\}$  for a ball we have followed the formulation in Tsang et al. [55]. In this work, it is shown that

$$\begin{aligned} \text{Asym}\{\mathbb{G}^{\text{vac}}\}(\mathbf{r}_a, \mathbf{r}'_a) &= k_o^3 \sum_{l=1}^{\infty} \sum_{m=-l}^l (-1)^m \\ & \sum_{j=1}^2 \mathbf{r} \mathbf{S}_{l,m}^{(j)}(r, \theta, \phi) \otimes \mathbf{r}' \mathbf{S}_{l,-m}^{(j)}(r', \theta', \phi') \end{aligned} \quad (23)$$

where

$$\begin{aligned} \mathbf{rS}_{lm}^{(1)}(r, \theta, \phi) &= \sqrt{\frac{2l+1}{4\pi l(l+1)}} j_l(r) \mathbf{V}_{lm}^{(3)}(\theta, \phi) \\ \mathbf{rS}_{lm}^{(2)}(r, \theta, \phi) &= \sqrt{\frac{2l+1}{4\pi l(l+1)}} \left( \frac{l(l+1)}{r} j_l(r) \mathbf{V}_{lm}^{(1)}(\theta, \phi) \right. \\ &\quad \left. + \frac{1}{r} \frac{d(r j_l(r))}{dr} \mathbf{V}_{lm}^{(2)}(\theta, \phi) \right). \end{aligned} \quad (24)$$

In these definition,  $\mathbf{V}_{lm}^{(\alpha)}$  are the vector spherical harmonics, obeying the orthogonality conditions

$$\begin{aligned} \int d\Omega \mathbf{V}_{lm}^{(\alpha)}(\theta, \phi) \mathbf{V}_{l'm'}^{(\beta)}(\theta, \phi) \\ = \delta_{\alpha, \beta} \delta_{m, m'} \delta_{l, l'} \begin{cases} (-1)^m \frac{4\pi}{2l+1}, & \alpha = 1 \\ (-1)^m \frac{4\pi l(l+1)}{2l+1}, & \alpha = \{2, 3\} \end{cases} \end{aligned} \quad (25)$$

(As the spherical harmonics are unaffected by projection into a connected volume, the program given below is also valid for shells and other homeomorphic domains.) Comparing (23) with a standard singular value decomposition, we equate the value of the inner product of the vector pairs forming the above outer products with the singular values of  $\text{Asym}\{\mathbb{G}^{\text{vac}}\}$ . Performing the angular integrals over the vector spherical harmonics, results in two types of singular values

$$\begin{aligned} \rho_{lm}^{(1)} &= \int_0^R dr r^2 j_l^2(r) \\ &= \frac{\pi R^2}{4} \left( j_{l+\frac{1}{2}}^2(R) - j_{l-\frac{1}{2}}^2(R) j_{l+\frac{3}{2}}(R) \right) \\ \rho_{lm}^{(2)} &= \int_0^R dr r^2 \left( \frac{l+1}{2l+1} j_{l-1}^2(r) + \frac{l}{2l+1} j_{l+1}^2(r) \right) \\ &= \frac{\pi R^2}{4} \left( \frac{l+1}{2l+1} \left( j_{l-\frac{1}{2}}^2(R) - j_{l+\frac{1}{2}}(R) j_{l-\frac{3}{2}}(R) \right) \right. \\ &\quad \left. + \frac{l}{2l+1} \left( j_{l+\frac{1}{2}}^2(R) - j_{l+\frac{5}{2}}(R) j_{l+\frac{3}{2}}(R) \right) \right) \end{aligned} \quad (26)$$

where each  $l$  index has a multiplicity of  $(2l+1)$  and  $R$  is the radius of the ball normalized by  $k_o = 2\pi/\lambda$ . For large values of  $R$ ,  $R \gg \left| (l \pm n/2)^2 - 1/4 \right|$ , each of these singular values begins to scale as  $\propto \pi R$ . For small arguments  $0 < R \ll \sqrt{l \pm n/2 + 1}$  the Bessel functions scale as

$$j_{l \pm n/2}(R) \propto \frac{\sqrt{\pi}}{2\Gamma\left(l + \frac{3 \pm n}{2}\right)} \left(\frac{R}{2}\right)^{l \pm n/2} \quad (27)$$

so that the  $l = 1$  term gives volumetric scaling. This asymptotic behaviour is the basis for the statement made in the main text that for a spherical bounding volume the

singular values display a tail that decays as geometric factors over factorials. Past some index, (27) is always a close approximation of the true value of the Bessel function, independent of the value of  $R$ .

To see that this asymptotic also implies sub-logarithmic scaling with  $\zeta$ , consider the first type of singular values in the limit of (27)

$$\rho_{lm}^{(1)} \approx \frac{\pi}{2^2} \left(\frac{R}{2}\right)^2 \frac{1}{(l+1)!(l+2)!}. \quad (28)$$

(The same analysis applies to the second type of singular values.) Suppose that  $\zeta = \rho_{lm}^{(1)}$ . Summing the remaining (unsaturated) linear term of (6) we then have

$$\begin{aligned} \sum_{l+1}^{\infty} (2l+1) \rho_{lm}^{(1)} \zeta &= \frac{r^2}{4(l+2)(l+3)} \\ &\left( (2l+1) \text{HypGeo} \left( 1, \{3+l, 4+l\}, \frac{R^2}{4} \right) \right. \\ &\quad \left. + 2 \text{HypGeo} \left( 1, \{3+l, 4+l\}, \frac{R^2}{4} \right) \right), \end{aligned} \quad (29)$$

where HypGeo is the generalized hypergeometric function. If  $\zeta$  is large then  $l$  will also be large, and (29) is both small and only weakly dependent on the value of  $l$ . Therefore, the growth in  $\Phi$  produced by growth in  $\zeta$  results, to increasingly good accuracy, from the contribution of the nearest unsaturated singular value. In this large  $l$  and  $\zeta$  limit, applying Sterling's approximation to (28) shows that the dependence of  $l$  on  $\zeta$  is

$$(2l+3) \left( \ln \left( \frac{2(l+1)}{R} \right) - 1 \right) = \ln(\zeta) - \ln \left( \frac{\pi}{2} \right), \quad (30)$$

where  $\ln(\dots)$  is the natural logarithm. The leading order terms of this expression give the stated scaling.

**Singular values for films**—Calculation of the singular values for films of thickness  $h$  follows a similar procedure to that of a ball. Using results from Tsang et al. [55] and Krüger et al. [41], the imaginary part of the Green function can generally be decomposed in terms of “regularized” spectral basis as  $\text{Asym}\{\mathbb{G}^{\text{vac}}\} = \sum_{j \in \text{prop}} |\mathbf{E}_j^{\text{reg}}\rangle \langle \mathbf{E}_j^{\text{reg}}|$ . The “propagating” basis functions of this set are orthogonal to one other (though not necessarily self-normalizable), and form a complete set both at the origin and at infinity. In particular, considering the in-plane wavevector  $\mathbf{k} = k_x \mathbf{e}_x + k_y \mathbf{e}_y \in \mathbb{R}^2$ , the basis functions can be written as plane waves  $\mathbf{E}_{s,p}^{\text{reg}}(\mathbf{k}, \mathbf{r})$ , with  $s \in \{-1, 1\}$  denoting the parity and  $p \in \{M, N\}$  the polarization. The vacuum Green function in this basis then takes on the form

$$\begin{aligned} \text{Asym}\{\mathbb{G}^{\text{vac}}\}(\mathbf{r}, \mathbf{r}') &= \\ \sum_{p,s} \int_{|\mathbf{k}| \leq k_o} \mathbf{E}_{s,p}^{\text{reg}}(\mathbf{k}, \mathbf{r}) \otimes \mathbf{E}_{s,p}^{\text{reg}*}(\mathbf{k}, \mathbf{r}') \frac{d^2k}{(2\pi)^2}, \end{aligned} \quad (31)$$

with singular vector functions given by

$$\begin{aligned}
\mathbf{E}_{+,M}^{\text{reg}}(\mathbf{k}, \mathbf{r}) &= \frac{ik_o e^{i(k_x x + k_y y)}}{\sqrt{2k_z}|\mathbf{k}|} (k_y \mathbf{e}_x - k_x \mathbf{e}_y) \cos(k_z z) \\
\mathbf{E}_{-,M}^{\text{reg}}(\mathbf{k}, \mathbf{r}) &= \frac{-ik_o e^{i(k_x x + k_y y)}}{\sqrt{2k_z}|\mathbf{k}|} (k_y \mathbf{e}_x - k_x \mathbf{e}_y) \sin(k_z z) \\
\mathbf{E}_{+,N}^{\text{reg}}(\mathbf{k}, \mathbf{r}) &= \frac{e^{i(k_x x + k_y y)}}{\sqrt{2k_z}|\mathbf{k}|} \left( |\mathbf{k}|^2 \cos(k_z z) \mathbf{e}_z \right. \\
&\quad \left. - ik k_z \sin(k_z z) \right) \\
\mathbf{E}_{-,N}^{\text{reg}}(\mathbf{k}, \mathbf{r}) &= \frac{e^{i(k_x x + k_y y)}}{\sqrt{2k_z}|\mathbf{k}|} \left( ik k_z \cos(k_z z) \right. \\
&\quad \left. - |\mathbf{k}|^2 \sin(k_z z) \mathbf{e}_z \right)
\end{aligned} \tag{32}$$

in position space, where  $k_z = \sqrt{k_o^2 - |\mathbf{k}|^2}$  is real and nonnegative by virtue of the restriction to propagating waves. The inner products may then all be written as

$$\langle \mathbf{E}_{s',p'}^{\text{reg}}(\mathbf{k}'), \mathbf{E}_{s,p}^{\text{reg}}(\mathbf{k}) \rangle = \rho_{s,p}(\mathbf{k}) (2\pi)^2 \delta^2(\mathbf{k} - \mathbf{k}') \delta_{s,s'} \delta_{p,p'} \tag{33}$$

due to the orthogonality of these basis functions. This immediately yields the desired singular values corresponding to each  $\mathbf{k}$ :

$$\begin{aligned}
\rho_{\pm,M}(\mathbf{k}) &= \frac{k_o^2 h}{4} \left( 1 \pm \frac{\sin(k_z h)}{k_z h} \right) \\
\rho_{\pm,N}(\mathbf{k}) &= \frac{k_o^2 h}{4k_z} \left( 1 \pm \frac{\sin(k_z h)}{k_z h} \right) \mp \frac{\sin(k_z h)}{2}.
\end{aligned} \tag{34}$$

**Scalar approximation for films**—Computation of the domain correlation factor (10) for the scalar approximation of a film of thickness  $h$  is most conveniently carried out by expressing the vacuum Green function in Fourier domain as

$$\begin{aligned}
&\text{Asym} \{ \mathbb{G}^{\text{vac}} \} (\mathbf{r}, \mathbf{r}') = \\
&\lim_{\eta \rightarrow 0} k_o^2 \int \frac{d^3 k}{(2\pi)^3} \frac{2k_o \eta e^{i\mathbf{k} \cdot (\mathbf{r} - \mathbf{r}')} (\mathbf{p} \otimes \mathbf{p}' + \mathbf{s} \otimes \mathbf{s}')}{(|\mathbf{k}|^2 - k_o^2 - i2k_o \eta) (|\mathbf{k}|^2 - k_o^2 + i2k_o \eta)},
\end{aligned} \tag{35}$$

with  $\mathbf{p}$  and  $\mathbf{s}$  denoting two orthogonal polarizations.

Skipping some straightforward but tedious integration details, one finds that in the limit that  $\eta \rightarrow 0$  the only contribution that does not vanish is

$$\begin{aligned}
&\iint d\mathbf{r} d\mathbf{r}' (\text{Asym} \{ \mathbb{G}^{\text{vac}}(\mathbf{r}, \mathbf{r}') \})^2 = A \iint_{-h/2}^{h/2} dz dz' \\
&\lim_{\eta \rightarrow 0} \int_0^\infty \frac{dk}{2} \frac{k}{|k_z|^2} \left( e^{2ik_z |z-z'|} + e^{-2ik_z^* |z-z'|} \right),
\end{aligned}$$

where we have defined  $k_z = \sqrt{|\mathbf{k}|^2 - k_o^2 + 2i\eta k_o}$ . Making the coordinate transformation  $u = k_z$ , the path of

integration is found to begin at  $u = 1$ , move towards the origin (approximately along the real axis), and then curve to asymptotically follow the imaginary axis toward  $\infty$ . In the limit  $\eta \rightarrow 0$ , normalizing by  $k_o$ , this path is described to arbitrary accuracy by integrating backwards from 1 to  $\sqrt{2\eta}$ , moving along a circular contour to  $\sqrt{2\eta}i$  and then proceeding along the imaginary axis. Explicitly, this leads to the integrals

$$\begin{aligned}
&\int_1^\infty du \frac{e^{-2u|z_1-z_2|}}{u} + \int_{\sqrt{2\eta}}^1 du \frac{e^{-2u|z_1-z_2|} - \cos(2u|z_1-z_2|)}{u} \\
&- i \int_0^{\pi/2} d\theta e^{-2\sqrt{2\eta}|z_1-z_2| \sin(\theta)} \cos\left(2\sqrt{2\eta}|z_1-z_2| \cos(\theta)\right).
\end{aligned} \tag{36}$$

The first and second contributions can be broken into known special functions, while the third can easily be handled with a numeric procedure in the limit. Evaluating these results over the remaining  $z$  coordinate integrals yields

$$\iint d\mathbf{r} d\mathbf{r}' (\text{Asym} \{ \mathbb{G}^{\text{vac}}(\mathbf{r}, \mathbf{r}') \})^2 = A c(h), \tag{37}$$

where  $c(h)$  is a function of the wavelength normalized thickness given by

$$\begin{aligned}
c(h) &= \frac{1 - \cos(2\pi h)}{4} + 2\pi h \sin(2\pi h) \cos(2\pi h) + \\
&(2\pi h)^2 \left( \frac{\pi}{2} - \text{CosInt}(4\pi h) \right)
\end{aligned} \tag{38}$$

In the large  $h$  limit,  $c(h)$  rapidly asymptotes to  $h^2$ .

**Inverse design**—To explore the largest possible design space, geometric optimization is carried out using the “topology” optimization approach [2], in which each pixel (permittivity value) within the chosen bounding domain is considered as an independent design parameter. The key to the tractability of such large-scale optimizations is the use of gradient-based optimization algorithms, such as the method of moving asymptotes [56]. To make use of these approaches, each pixel is initially treated as continuous, and then subsequently binarized with filter and regularization methods [51].

The primary challenge of the inverse design problem lies in the expensive evaluation of  $\Phi$  for inhomogeneous medium, which may be evaluated thousands of times in a typical optimization routine. To surmount this difficulty, we exploit our previous fluctuating volume current formulation [47, 57]. This framework both removes any unknown outside of the bounding domain, and allows the central matrix-vector multiplication,  $\mathbb{G}^{\text{vac}} \mathbf{J}$ , to be computed via the fast-Fourier transform. To further reduce

computational cost we also use the fact that  $\text{Asym}\{\mathbb{G}^{\text{vac}}\}$  is low-rank. This allows the singular value decomposition (SVD)  $\text{Asym}\{\mathbb{G}^{\text{vac}}\} = U\Sigma U^\dagger$  to be approximated to any accuracy with an efficient randomized method [58], resulting in a tall-and-skinny matrix  $U \in \mathbb{R}^{N \times n}$  and a small matrix  $\Sigma \in \mathbb{R}^{n \times n}$ , where  $n \ll N$  [47]. Starting from an alternative (equivalent) trace form of (2), we then have

$$\begin{aligned} \Phi &= \frac{2}{\pi} \text{Tr} \{ \text{Asym} \{ \mathbb{V} \} |\mathbb{V}|^{-2} \mathbb{T}^\dagger \text{Asym} \{ \mathbb{G}^{\text{vac}} \} \mathbb{T} \} \\ &= \frac{2}{\pi} \| \sqrt{\text{Asym} \{ \mathbb{V} \}} \mathbb{V}^{-1} \mathbb{T}^\dagger U \sqrt{\Sigma} \|_F^2. \end{aligned} \quad (39)$$

Evaluation of (39) requires only one inverse solve for each column  $U_i$  (r total):

$$\mathbb{T}^{\dagger-1} Q_i = (\mathbb{V}^{\dagger-1} - \mathbb{G}^{\text{vac}\dagger}) Q_i = U_i. \quad (40)$$

(39) is also well suited to calculation of the gradient of  $\Phi$ . Setting the susceptibility at the  $i$ -th pixel by the linear equation  $\chi_i = \chi p_i$ , with  $p_i \in [0, 1]$  the design parameter and  $\chi$  the susceptibility of the material, direct application of matrix calculus shows that

$$\partial_{p_i} \mathbb{T} = -\mathbb{T} \partial_{p_i} \chi_i^{-1} \delta_{i,i} \mathbb{T}. \quad (41)$$

Using this result the total gradient is then

$$\begin{aligned} \partial_{p_i} \Phi &= \frac{2}{\pi} \left( \partial_{p_i} \frac{\text{Im}(\chi_\alpha)}{|\chi_\alpha|^2} \right) (\mathbb{T}^\dagger U \Sigma U^\dagger \mathbb{T})_{i,i} \\ &+ \frac{4}{\pi} \text{Re} \left( (\partial_{p_i} \chi_i^{-1*}) \mathbb{T}^\dagger U \Sigma U^\dagger \mathbb{T} |\mathbb{V}|^{-2} \text{Im}(\mathbb{V}) \mathbb{T}^\dagger \right)_{i,i}. \end{aligned} \quad (42)$$

As before, only  $n$  solves are required to evaluate (42) for all design parameters.

**Singular values of  $\mathbb{T}$  from inverse design**—As a point of comparison with the assumptions made in deriving (6), we have explored the representation of the  $\mathbb{T}$  operator for the dielectric structure of the rightmost black squares ( $\chi = 20 + 4i$ ,  $\Phi = 0.6 \Phi_{\text{opt}}$ ) in the basis of  $\text{Asym}\{\mathbb{G}^{\text{vac}}\}$ . This physical realizations prove to nearly satisfy both the assumption of asymmetry ( $\text{atan}(\text{Im}(\langle \mathbf{q}_i | \mathbb{T} | \mathbf{q}_i \rangle)) / \text{Re}(\langle \mathbf{q}_i | \mathbb{T} | \mathbf{q}_i \rangle) = \pi/2$ ) and simultaneous diagonalizability, as we find that

$$\sqrt{\sum_i \text{Im}(\langle \mathbf{q}_i | \mathbb{T} | \mathbf{q}_i \rangle)^2} / \sqrt{\sum_{i,j} |\langle \mathbf{q}_i | \mathbb{T} | \mathbf{q}_j \rangle|^2} = 0.97.$$

The ratio of the true values of  $\langle \mathbf{q}_i | \mathbb{T} | \mathbf{q}_i \rangle$  in comparison to the ideal values determined by (6) are given in Tab.1 below. These values are naturally grouped by a singular value type index ( $\{1, 2\}$ ) and the spherical harmonic “ $l$ ” index. For clarity, an average is taken over the (ideally constant) harmonic “ $m$ ” subindex, and the final column gives the weight that each entry makes to  $\Phi_{\text{opt}}$ . (This is same notation used in discussing the singular values for a ball.)

$l$ -Type	Ideal Value	Average Ratio	Weight
1 – 1	0.32	0.94	0.05
1 – 2	0.40	1.32	0.05
2 – 1	0.81	1.29	0.08
2 – 2	0.50	1.19	0.08
3 – 1	4.18	0.83	0.11
3 – 2	1.40	0.67	0.11
4 – 1	36.25	0.53	0.13
4 – 2	7.48	0.60	0.13
5 – 2	66.23	0.04	0.17

TABLE I. **Comparison of  $\mathbb{T}$  response values for exemplary structure.** Comparison of the values of  $|\langle \mathbf{q}_i | \mathbb{T} | \mathbf{q}_i \rangle|$  (where  $\mathbf{q}_i$  are the singular vectors of  $\text{Asym}\{\mathbb{G}^{\text{vac}}\}$ ) for the structure of the rightmost black square,  $\chi = 20 + 4i$  ( $\zeta = 104$ ), of Fig. 3 to the magnitude of the ideal values set by (6). Although the two set values agree to great extent, pronounced differences between the ideal response dictated bound and the  $\mathbb{T}$  operators of the optimized structures are seen for higher spherical harmonics  $l$ -numbers when the magnitude of ideal value of  $\langle \mathbf{q}_i | \mathbb{T} | \mathbf{q}_i \rangle$  approaches  $\zeta$ .

- [1] A. F. Koenderink, A. Alu, and A. Polman, *Science* **348**, 516 (2015).
- [2] S. Molesky, Z. Lin, A. Y. Piggott, W. Jin, J. Vucković, and A. W. Rodriguez, *Nature Photonics* **12**, 659 (2018).
- [3] P. Du and J. S. Yu, *Chemical Engineering Journal* **327**, 109 (2017).
- [4] J. K. Tong, W.-C. Hsu, Y. Huang, S. V. Boriskina, and G. Chen, *Scientific Reports* **5**, 10661 (2015).
- [5] L. Zhu, A. P. Raman, and S. Fan, *Proceedings of the National Academy of Sciences* **112**, 12282 (2015).
- [6] O. Ilic, P. Bermel, G. Chen, J. D. Joannopoulos, I. Celanovic, and M. Soljačić, *Nature Nanotechnology* **11**, 320 (2016).
- [7] C. F. Bohren and D. R. Huffman, *Absorption and scattering of light by small particles* (John Wiley & Sons, 2008).
- [8] M. I. Tribelsky, *Europhysics Letters* **94**, 14004 (2011).
- [9] Z. Ruan and S. Fan, *Applied Physics Letters* **98**, 043101 (2011).
- [10] S.-A. Biehs and P. Ben-Abdallah, *Physical Review B* **93**, 165405 (2016).
- [11] V. Fernández-Hurtado, A. I. Fernández-Domínguez, J. Feist, F. J. García-Vidal, and J. C. Cuevas, *Physical Review B* **97**, 045408 (2018).
- [12] D. Thompson, L. Zhu, R. Mittapally, S. Sadat, Z. Xing, P. McArdle, M. M. Qazilbash, P. Reddy, and E. Meyhofer, *Nature* **561**, 216 (2018).
- [13] M. A. Kats and F. Capasso, *Laser & Photonics Reviews* **10**, 735 (2016).
- [14] P. N. Dyachenko, S. Molesky, A. Y. Petrov, M. Störmer, T. Krekeler, S. Lang, M. Ritter, Z. Jacob, and M. Eich, *Nature Communications* **7**, 11809 (2016).
- [15] V. Dolores-Calzadilla, B. Romeira, F. Pagliano, S. Birindelli, A. Higuera-Rodriguez, P. Van Veldhoven, M. Smit, A. Fiore, and D. Heiss, *Nature Communications* **8**, 14323 (2017).

- [16] S.-i. Inoue, N. Tamari, and M. Taniguchi, *Applied Physics Letters* **110**, 141106 (2017).
- [17] E. Yablonovitch, *JOSA* **72**, 899 (1982).
- [18] H. A. Atwater and A. Polman, *Nature Materials* **9**, 205 (2010).
- [19] D. Jariwala, A. R. Davoyan, J. Wong, and H. A. Atwater, *ACS Photonics* **4**, 2962 (2017).
- [20] J. D. Thompson, T. Tietze, N. P. de Leon, J. Feist, A. Akimov, M. Gullans, A. S. Zibrov, V. Vuletić, and M. D. Lukin, *Science* **340**, 1202 (2013).
- [21] T. Galfsky, H. Krishnamoorthy, W. Newman, E. Nari-manov, Z. Jacob, and V. Menon, *Optica* **2**, 62 (2015).
- [22] N. Somaschi, V. Giesz, L. De Santis, J. Loredano, M. P. Almeida, G. Hornecker, S. L. Portalupi, T. Grange, C. Antón, J. Demory, C. Gómez, I. Sagnes, N. D. Lanzillotti-Kimura, A. Lemaître, A. Auffeves, A. G. White, L. Lanco, and P. Senellart, *Nature Photonics* **10**, 340 (2016).
- [23] J. S. McLean, *IEEE Transactions on Antennas and Propagation* **44**, 672 (1996).
- [24] R. E. Hamam, A. Karalis, J. Joannopoulos, and M. Soljačić, *Physical Review A* **75**, 053801 (2007).
- [25] D.-H. Kwon and D. M. Pozar, *IEEE Transactions on Antennas and Propagation* **57**, 3720 (2009).
- [26] Z. Yu, A. Raman, and S. Fan, *Proceedings of the National Academy of Sciences* **107**, 17491 (2010).
- [27] Z. Yu, A. Raman, and S. Fan, *Optics Express* **18**, A366 (2010).
- [28] Z. Ruan and S. Fan, *Physical Review Letters* **105**, 013901 (2010).
- [29] J.-P. Hugonin, M. Besbes, and P. Ben-Abdallah, *Physical Review B* **91**, 180202 (2015).
- [30] Y. Jia, M. Qiu, H. Wu, Y. Cui, S. Fan, and Z. Ruan, *Nano Letters* **15**, 5513 (2015).
- [31] Y. Yang, O. D. Miller, T. Christensen, J. D. Joannopoulos, and M. Soljačić, *Nano Letters* **17**, 3238 (2017).
- [32] D. M. Callahan, J. N. Munday, and H. A. Atwater, *Nano letters* **12**, 214 (2012).
- [33] O. D. Miller, A. G. Polimeridis, M. H. Reid, C. W. Hsu, B. G. DeLacy, J. D. Joannopoulos, M. Soljačić, and S. G. Johnson, *Optics Express* **24**, 3329 (2016).
- [34] R. Fuchs and S. Liu, *Physical Review B* **14**, 5521 (1976).
- [35] O. D. Miller, C. W. Hsu, M. H. Reid, W. Qiu, B. G. DeLacy, J. D. Joannopoulos, M. Soljačić, and S. G. Johnson, *Physical review letters* **112**, 123903 (2014).
- [36] H. Shim, L. Fan, S. G. Johnson, and O. D. Miller, *Physical Review X* **9**, 011043 (2019).
- [37] Z. Ruan and S. Fan, *Physical Review A* **85**, 043828 (2012).
- [38] F. Alpegiani, N. Parappurath, E. Verhagen, and L. Kuipers, *Physical Review X* **7**, 021035 (2017).
- [39] C. Sohl, M. Gustafsson, and G. Kristensson, *Journal of Physics D: Applied Physics* **40**, 7146 (2007).
- [40] M. Gustafsson, C. Sohl, and G. Kristensson, *Proceedings of the Royal Society A: Mathematical, Physical and Engineering Sciences* **463**, 2589 (2007).
- [41] M. Krüger, G. Bimonte, T. Emig, and M. Kardar, *Physical Review B* **86**, 115423 (2012).
- [42] J.-J. Greffet and M. Nieto-Vesperinas, *JOSA A* **15**, 2735 (1998).
- [43] S. Molesky, P. S. Venkataram, W. Jin, and A. W. Rodriguez, *arXiv preprint arXiv:1907.03000*, 12 (2019).
- [44] J. Pendry, *Journal of Physics A: Mathematical and General* **16**, 2161 (1983).
- [45] J. Pendry, *Journal of Physics: Condensed Matter* **11**, 6621 (1999).
- [46] A. G. Polimeridis, F. Vipiana, J. R. Mosig, and D. R. Wilton, *IEEE Transactions on Antennas and Propagation* **61**, 3112 (2013).
- [47] A. G. Polimeridis, M. Reid, W. Jin, S. G. Johnson, J. K. White, and A. W. Rodriguez, *Physical Review B* **92**, 134202 (2015).
- [48] S. Thongrattanasiri, F. H. Koppens, and F. J. G. De Abajo, *Physical Review Letters* **108**, 047401 (2012).
- [49] G. M. Akselrod, J. Huang, T. B. Hoang, P. T. Bowen, L. Su, D. R. Smith, and M. H. Mikkelsen, *Advanced Materials* **27**, 8028 (2015).
- [50] J. Nong, H. Da, Q. Fang, Y. Yu, and X. Yan, *Journal of Physics D: Applied Physics* **51**, 375105 (2018).
- [51] J. S. Jensen and O. Sigmund, *Laser & Photonics Reviews* **5**, 308 (2011).
- [52] E. D. Palik, *Handbook of optical constants of solids*, Vol. 3 (Academic Press, 1998).
- [53] B. A. Lippmann and J. Schwinger, *Physical Review* **79**, 469 (1950).
- [54] J. A. Kong, *Proceedings of the IEEE* **60**, 1036 (1972).
- [55] L. Tsang, J. A. Kong, and K.-H. Ding, *Scattering of electromagnetic waves: theories and applications*, Vol. 27 (John Wiley & Sons, 2004).
- [56] K. Svanberg, *SIAM Journal on Optimization* **12**, 555 (2002).
- [57] W. Jin, A. G. Polimeridis, and A. W. Rodriguez, *Physical Review B* **93**, 121403 (2016).
- [58] A. Hochman, J. Fernandez Villena, A. G. Polimeridis, L. M. Silveira, J. K. White, and L. Daniel, *IEEE Transactions on Antennas and Propagation* **62**, 3150 (2014).